Charge transfer and symmetry reduction at the CuPc/Ag(110) interface studied by photoemission tomography

K. Schönauer,[1,2,*] S. Weiss,[1,2] V. Feyer,[2,3] D. Lüftner,[4] B. Stadtmüller,[1,2,†] D. Schwarz,[1,2] T. Sueyoshi,[1,2,‡] C. Kumpf,[1,2] P. Puschnig,[4] M. G. Ramsey,[4] F. S. Tautz,[1,2] and S. Soubatch[1,2,§]

[1]*Peter Grünberg Institut (PGI-3), Forschungszentrum Jülich, 52425 Jülich, Germany*

[2]*Jülich Aachen Research Alliance (JARA), Fundamentals of Future Information Technology, 52425 Jülich, Germany*

[3]*Peter Grünberg Institut (PGI-6), Forschungszentrum Jülich, 52425 Jülich, Germany*

[4]*Institute of Physics, NAWI Graz, Karl-Franzens University Graz, 8010 Graz, Austria*

(Received 13 September 2016; revised manuscript received 4 November 2016; published 28 November 2016)

On the Ag(110) surface copper phthalocyanine (CuPc) orders in two structurally similar superstructures, as revealed by low-energy electron diffraction. Scanning tunneling microscopy (STM) shows that in both superstructures the molecular planes are oriented parallel to the surface and the long molecular axes, defined as diagonals of the square molecule, are rotated by $\simeq \pm 32^\circ$ away from the high-symmetry directions [1$\bar{1}$0] and [001] of the silver surface. Similarly to many other adsorbed metal phthalocyanines, the CuPc molecules on Ag(110) appear in STM as crosslike features with twofold symmetry. Photoemission tomography based on angle-resolved photoemission spectroscopy reveals a charge transfer from the substrate into the molecule. A symmetry analysis of experimental and theoretical constant binding energy maps of the photoemission intensity in the k_x,k_y-plane points to a preferential occupation of one of the two initially degenerate lowest unoccupied molecular orbitals (LUMOs) of e_g symmetry. The occupied e_g orbital is rotated by 32° against the [001] direction of the substrate. The lifting of the degeneracy of the LUMOs and the related reduction of the symmetry of the adsorbed CuPc molecule are attributed to an anisotropy in the chemical reactivity of the Ag(110) surface.

DOI: 10.1103/PhysRevB.94.205144

I. INTRODUCTION

Among other classes of organic semiconductors, phthalocyanines (Pc) have been studied intensively in recent years. Phthalocyanines are macrocycles with extended π conjugation, bringing about strong light absorption in the visible range. At the same time, their planar geometry and their thermal stability make them suitable for organic molecular beam epitaxy, and their ability to form complexes with many metals in the periodic table endows them with chemical versatility. This remarkable combination of properties makes these pigment molecules interesting for a large number of optoelectronic applications [1].

The chemical structure of copper phthalocyanine (CuPc) is displayed in Fig. 1(a). Four isoindole units are linked via nitrogen (aza-)bridges, resulting in tetrabenzoporphyrazine or phthalocyanine (2HPc), and in the central position of this macrocycle two hydrogen atoms are replaced by a single copper atom which forms coordination bonds with the four nitrogen atoms of the isoindole units.

The planarity of many metal phthalocyanine (MPc) molecules implies that the metal center is accessible from both sides of the molecular plane [1]. In particular, adsorbed MPc molecules can interact via their metal atoms with the substrate, if they adsorb with the molecular plane parallel to it. However, in the case of Cu as a central metal atom, this interaction is expected to be weak, because the Cu d shell is completely filled. There remains, however, the conjugated π-electron system in the macrocycle which can interact either chemisorptively or physisorptively with the metal substrate. This can lead to charge transfer from the metal into the lowest unoccupied molecular orbital (LUMO).

In this paper, we investigate this charge transfer more closely. While as such charge transfer is not uncommon (e.g., [2–4] and others), in the present case it raises an intriguing question, arising from the particular electronic structure of the phthalocyanines. Density functional theory (DFT) calculations reveal that "the LUMO" of gas-phase CuPc [5,6] and many other related molecules is doubly degenerate and belongs to the e_g representation of the D_{4h} symmetry group of the free molecule. Figures 1(b) and 1(c) display the two corresponding orbitals. They show that in each of the two orbitals the probability amplitude is concentrated on opposite isoindole units (IIUs), while the two remaining IIUs show substantially reduced wave function amplitudes. The question thus arises whether the charge transfer from the metal is directed equally into the two e_g orbitals, or whether their degeneracy is lifted and one of the two receives more charge from the substrate.

We note that the degeneracy of the LUMO is closely related to cross-conjugation in the central porphyrazine macrocycle of phthalocyanines. Cross-conjugation is given when in a set of three π bonds only two π bonds interact with each other by conjugation, while the third one is excluded from interaction [7]. As a result of the cross-conjugation at the vertices of the aza-bridges and the pyrrole units in the porphyrazine macrocycle, two cyclic paths of alternating

*Present address: Institut für Energie- und Klimaforschung, Forschungszentrum Jülich, 52425 Jülich, Germany.

†Present address: Department of Physics and Research Center OPTIMAS, University of Kaiserslautern, 67663 Kaiserslautern, Germany.

‡Present address: Institut für Experimentelle und Angewandte Physik, Christian-Albrechts-Universität zu Kiel, 24098 Kiel, Germany.

§Corresponding author: s.subach@fz-juelich.de

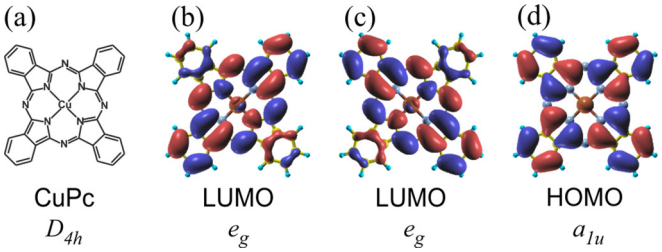

FIG. 1. CuPc molecule and its frontier orbitals according to DFT calculation: (a) chemical structure; (b), (c) degenerate LUMOs, e_g symmetry; (d) highest occupied molecular orbital (HOMO), a_{1u} symmetry.

single and double bonds, each involving 18 electrons, can be drawn in the chemical structure formula of CuPc [1]. Two pyrrole units at opposite ends of the molecules are included within each of these paths, while the remaining two are not. As a consequence, there exist two distinct tautomeric 18-electron paths of alternating single and double bonds. Because the lobular structure of the LUMO closely reflects these cyclic paths, two degenerate "tautomeric" orbitals must also exist, which together transform according to the two-dimensional e_g representation. In fact, the cross-conjugation in CuPc can be easily spotted in the real-space plots of the LUMO orbitals in Figs. 1(b) and 1(c), as in each of the two orbitals two opposing benzene rings of the isoindole units harbor benzene-like π orbitals that are separated from the rest of the molecule, while the other two benzene rings are well integrated into the lobular structure centered on the porphyrazine macrocycle.

Lifting the degeneracy and preferential occupation of one of the e_g orbitals should in principle lead to a symmetry breaking of the molecule on the surface, from a fourfold symmetric molecule-substrate complex (C_{4v}) to a twofold one (C_{2v}). Indeed, such symmetry reductions have been reported for several MPc molecules with scanning tunneling microscopy (STM) imaging, e.g., CoPc, CuPc, and FePc on Cu(111) [8], CuPc/Cu(111) [9], CoPc/Cu(111) [10,11], and SnPc/Ag(111) [12]. However, in conventional constant-current STM such a symmetry breaking could also result from a purely structural distortion, without essentially lifting the e_g degeneracy [13]. Indeed, in Refs. [8,11] the twofold symmetry of STM images was explained as a direct consequence of a substrate-induced molecular distortion. For example, for CoPc/Cu(111) the IIUs along one molecular axis come 0.2 Å closer to the surface than the other IIUs [11]. In contrast, in Ref. [9] degeneracy lifting has been mentioned as the possible origin of symmetry breaking for CuPc/Cu(111).

Thus, constant-current STM is generally not conclusive with regard to possible degeneracy lifting [14]. Moreover, because of the substrate-induced broadening of molecular energy levels it has to our knowledge never been possible to observe a splitting of the e_g LUMO resonance in scanning tunneling spectroscopy (STS) [15]. For this reason, complementary methods, such as density functional calculations, are often employed. For example, based on DFT calculations the symmetry breaking of the FePc STM contrast on Cu(111) was attributed to a cooperative effect of asymmetric downward bending and different charge transfer into the two isoindole pairs [14].

Electron spectroscopy, of course, offers the possibility to probe the electronic levels directly. Indeed, for CuPc and F_{16}CuPc on Ag(111) evidence for degeneracy lifting and preferential charge transfer from the surface into one orbital has been obtained from correspondingly split features in x-ray absorption and C1s core level spectra [16]. Lifting of degeneracy was assigned in this case to a Jahn-Teller mechanism [16]. Broadening of C1s and N1s levels has also been observed for FePc/Cu(111) [14] and been associated with the symmetry breaking observed in this system. In contrast, angle-resolved photoelectron spectroscopy (ARPES) for FePc/Ag(111) has shown no evidence for degeneracy lifting and preferential charge transfer within the experimental energy resolution (0.15 eV) [17].

Finally, it should be noted that in the special case of single, charged CuPc molecules on a bilayer of NaCl on Cu(111) the $C_{4v} \rightarrow C_{2v}$ symmetry breaking in STM images was conclusively assigned to degeneracy lifting (of the order of 0.2 eV) of the LUMO. In this case it was even possible to exclude a low-symmetry adsorption geometry as the origin and trace it instead to a Jahn-Teller effect within the molecule [15]. Principally, degeneracy lifting can have two origins. On the one hand, it can be induced by the external environment, e.g., by a low-symmetry adsorption site as the result of which the two orbitals interact differently with the substrate. This mechanism may be accompanied by an externally forced distortion of the molecule. On the other hand, in a Jahn-Teller scenario [18] the occupation of only one of the initially degenerate orbitals generates an internal distortion of the molecule that in turn lifts the degeneracy and thus stabilizes the preferential occupation. This mechanism can occur in a completely symmetric environment.

Because of the generally unsettled state of affairs as detailed above, we revisit here the longstanding question regarding the origin of the observed symmetry breaking and its possible relation to a lifting of the LUMO degeneracy, a preferential charge transfer, and molecular distortions. We employ a particular variant of ARPES, the so-called orbital or photoemission tomography (PT) [19,20]. Within the plane wave approximation, PT allows direct imaging of the orbital structure in k space, because the angular distribution of photoelectrons reflects the Fourier transform of the real-space orbital. We have selected the CuPc/Ag(110) system for our experiments. The choice of Cu as a central atom is motivated by its small interaction with the substrate; thus, the relative importance of the π-conjugated system in the interaction with the substrate is maximized. The choice of the Ag(110) substrate, on the other hand, is determined by the fact that on this anisotropic surface all CuPc molecules in the unit cell exhibit a single in-plane orientation, making the tomography analysis as straightforward as possible. We find that the two LUMO orbitals are occupied unevenly, with the one oriented 32° against the [001] direction of the substrate receiving more charge from the surface. This implies the lifting of the degeneracy. Interestingly, previous attempts to apply PT to MPc adsorption showed that for FePc on Ag(100), Ag(110), and Ag(111) both LUMOs are occupied equally [17].

The advantage of PT over many other approaches to analyze the origin of symmetry breaking is that not only can degeneracy lifting and partial filling of electronic states be observed

directly, but also the orientation of the newly filled orbital be determined unambiguously, at least if not too many differently oriented molecules are present at the surface. When multiple orientations are present and PT becomes difficult, it is desirable to have spectroscopic methods available in which the lateral orientation does not play a role in the analysis. Vibrational spectroscopy is one such method, as we demonstrate in Ref. [21], where PtPc/Ag(111) and PdPc/Ag(111) have been studied and, similarly to the present case, a lifting of the degeneracy of the two LUMOs is found.

The paper is organized as follows. We start with an investigation of the structure of CuPc/Ag(110). Then we demonstrate that constant-current STM images show a strong symmetry breaking of the CuPc molecules, while, as typically observed, STS is not able to resolve two separate orbitals on the energy axis. Then we present our PT experiments and finally relate the results of the electronic analysis to structural aspects of CuPc/Ag(110).

II. EXPERIMENTAL AND CALCULATION DETAILS

The sample preparation and all measurements were carried out in ultrahigh-vacuum vessels with a pressure of better than 10^{-9} mbar. Ag(110) crystals were cleaned in the conventional way by several cycles of sputtering and annealing. To obtain a compact and ordered monolayer of CuPc/Ag(110) as required for STM/STS and PT measurements, a few layers of CuPc were deposited onto the clean metal surface and the excess of the material was subsequently removed by thermal desorption at 600 K.

The structure of the layer was controlled with low-energy electron diffraction (LEED). Diffraction patterns were recorded at room temperature. Depending on the experiment, a conventional LEED, a micro-channel-plate (MCP-)LEED (OCI Vacuum Microengineering Inc.), or an Omicron spot profile analysis (SPA-)LEED was employed. Analysis of the LEED data and the unit cell optimization were done with the Spot-Plotter software [22]. In all cases we found equivalent diffraction patterns, which demonstrates the reproducibility of our preparation procedure. STM and STS experiments were performed with a Pt-Ir tip at temperatures below 10 K in a CreaTec Fischer & Co. GmbH microscope. Synchrotron-based ARPES experiments were carried out at Elettra Sincrotrone in Trieste, Italy. The NanoESCA beamline is equipped with a photoemission electron microscope (PEEM) from Omicron NanoTechnology GmbH [23]. Operated in momentum mode, the PEEM detects angle-resolved photoemission intensities in the whole emission hemisphere above the sample surface. PT measurements were performed at room temperature with a photon energy of 35 eV. The incidence angle of the p-polarized light was 65° with respect to the surface normal. The sample was oriented such that the photon beam, the sample normal, and the $[1\bar{1}0]$ direction of Ag were lying in the same plane, with the sample normal directed along the electron-optical axis of the microscope.

DFT calculations of gas-phase CuPc molecules were carried out within the generalized gradient approximation (GGA) [24] with the plane wave code ABINIT [25]. A supercell approach with a vacuum slab of at least $\simeq$15 Å width between CuPc molecules in each direction was employed. The all-electron potentials were replaced by extended norm-conserving, highly transferable Troullier-Martins pseudopotentials [26], using a plane wave cutoff of 50 Ryd. Following Refs. [19,20], reciprocal-space photoemission maps were simulated.

III. RESULTS AND DISCUSSION

A. Structural properties: Interplay of forces

We start by analyzing the structure of CuPc/Ag(110). As for many other phthalocyanines, a dilute disordered lattice gas in which molecules maximize their mutual distances is observed at low coverages. The reason for this behavior is intermolecular repulsion. However, at coverages slightly below one monolayer order sets in.

The LEED image of a compact CuPc monolayer is displayed in Fig. 2(a). A thorough analysis shows that the observed pattern consists of two distinct superstructures, labeled α and β [27]. The simulated patterns based on real-space vectors $\boldsymbol{b}_{1\alpha}$ and $\boldsymbol{b}_{2\alpha}$ of the α superstructure and $\boldsymbol{b}_{1\beta}$ and $\boldsymbol{b}_{2\beta}$ of the β superstructure are marked in Fig. 2(a) by solid and open circles, respectively. Only if both simulated LEED patterns are superimposed, all diffraction spots can be accounted for. Moreover, the complete reconstruction of the experimental LEED pattern requires the existence of one mirror domain for each of the two superstructures. This is the consequence of the symmetry group of the substrate.

The unit cell vectors of the α and β superstructures are specified in Table I. The corresponding optimized superstructure matrices are

$$M_\alpha = \begin{pmatrix} 3.00 \pm 0.05 & 1.72 \pm 0.08 \\ -1.77 \pm 0.05 & 4.00 \pm 0.06 \end{pmatrix}$$

and

$$M_\beta = \begin{pmatrix} 2.76 \pm 0.04 & 2.26 \pm 0.07 \\ -1.77 \pm 0.05 & 4.00 \pm 0.06 \end{pmatrix}.$$

Following the classification by Hooks *et al.* [28], both superstructures exhibit only a weak degree of registry with the substrate lattice. This limits the capability of DFT to predict the presence or absence of charge transfer at the interface, which is essential in the context of this work.

Comparing the optimized parameters of the superstructures to each other, we find that their real-space vectors $\boldsymbol{b}_{2\alpha}$ and $\boldsymbol{b}_{2\beta}$ are the same, $\boldsymbol{b}_{2\alpha} = \boldsymbol{b}_{2\beta} = \boldsymbol{b}_2$. Moreover, their unit cells have nearly the same area (176.8 ± 5.8 Å^2 for α vs 176.7 ± 5.4 Å^2 for β). From the sizes of the unit cells, it is also clear that they cannot contain more than one CuPc molecule each. Hence, the decisive difference between superstructures α and β cannot be their packing density.

The coexistence of two different superstructures at the surface has the potential to complicate the PT analysis, if the orientations of molecules in the two unit cells differ. However, our STM study reveals that in both superstructures CuPc molecules have the same orientation within experimental uncertainties. In Fig. 2(b) an STM image is displayed in which all supercell vectors can be recognized and the characteristic crosslike shape of the CuPc molecules can be distinguished. The long molecular axes, defined as diagonals of the square

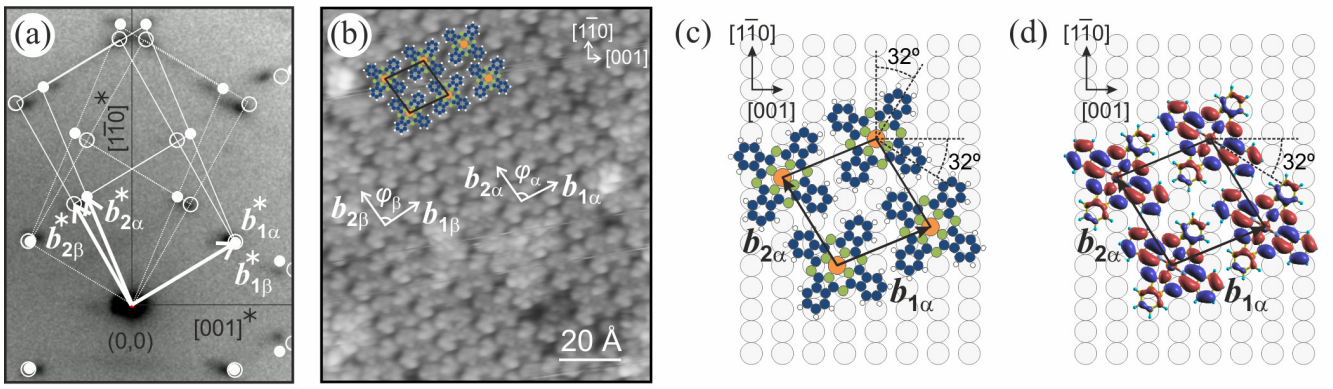

FIG. 2. Ordered monolayer of CuPc on Ag(110). (a) SPA-LEED image taken at 30 eV electron energy (raw data, no distortion correction) and simulated LEED patterns for two lattices formed by two pairs of unit cell vectors in reciprocal space: ($\boldsymbol{b}^*_{1\alpha}$, $\boldsymbol{b}^*_{2\alpha}$), solid white dots; ($\boldsymbol{b}^*_{1\beta}$, $\boldsymbol{b}^*_{2\beta}$), open white circles. (b) Low-temperature STM image ($U = -0.2$ V, $I = 30$ pA) with the unit cell vectors ($\boldsymbol{b}_{1\alpha}$, $\boldsymbol{b}_{2\alpha}$) and ($\boldsymbol{b}_{1\beta}$, $\boldsymbol{b}_{2\beta}$) of the two differently ordered superstructures. (c) Structural model of the unit cell of the α superstructure. (d) Same as in panel (c) with the LUMO$^{[001]}$ shown.

molecule, are rotated by $\simeq 32^\circ$ away from the high-symmetry directions [1$\bar{1}$0] and [001] of the silver surface [Fig. 2(c)]. According to this STM image, the difference in the molecular packing is a translation of molecules along rows nearly parallel to the vector $\boldsymbol{b}_2$.

To analyze the coexistence of the two superstructures in more detail, we employ pair potential calculations of intermolecular interactions. In this approach the interaction between neighboring molecules is approximated by pairwise interactions, electrostatic and van der Waals, between all of their atoms [29]. Note that any interaction with the substrate is ignored in the framework of this approach. Despite this being a rough approximation, the method was found to be helpful to understand lateral structures of several molecule-metal interfaces [29–31].

The result of this calculation for a pair of two molecules of equal orientation is displayed in Fig. 3, where the intermolecular interaction energy Φ is plotted as a function of the relative x and y coordinates of the molecular centers [i.e., one of the molecules is fixed at the (0,0) position]. One sees that the lattice vector $\boldsymbol{b}_2$ (or, equivalently, $-\boldsymbol{b}_2$) places the second molecule (i.e., the molecule in the neighboring unit cell along the lattice translations $\pm\boldsymbol{b}_2$) close to a minimum of the intermolecular potential energy. Likewise, the vector $\boldsymbol{b}_{1\beta}$ points toward an equivalent minimum of the interaction energy, in contrast to $\boldsymbol{b}_{1\alpha}$, which is directed at a repulsive region. Thus, intermolecular interactions favor the β superstructure of CuPc, because all its molecules are located at (or close to) potential minima corresponding to a weak intermolecular attraction. In contrast, in the α superstructure only the molecules translated along the $\pm\boldsymbol{b}_2$ lattice vectors attract each other, while pairs of molecules along $\boldsymbol{b}_{1\alpha}$ experience repulsion.

We note that, in spite of the fact that the intermolecular interaction favors the β superstructure, upon cooling to low temperatures (<10 K) most of the CuPc monolayer on Ag(110) is found in the α superstructure [see, e.g., Fig. 2(b)], with the β superstructure appearing only at the boundaries of extended α domains. From the point of view of thermodynamics, this implies that $F_\alpha < F_\beta$, or in the $T \to 0$ limit $U_\alpha < U_\beta$, where F and U are the Helmholtz free and the internal energies of the corresponding superstructures. Considering the internal energy of each superstructure to be a sum of two terms attributed to the intermolecular interactions and the molecule-substrate interactions, $U_{\alpha,\beta} = U^{m\leftrightarrow m}_{\alpha,\beta} + U^{m\leftrightarrow s}_{\alpha,\beta}$, and taking into account that $U^{m\leftrightarrow m}_{\alpha} > U^{m\leftrightarrow m}_{\beta}$ as the pair potential calculations

TABLE I. Optimized structural parameters of the ordered monolayer of CuPc on Ag(110).

	length (Å)	angle to Ag[001] (°)	angle to $\boldsymbol{b}_2$ (°)
$\boldsymbol{b}_{1\alpha}$	13.2 ± 0.2	22 ± 1	100 ± 1
$\boldsymbol{b}_2$	13.6 ± 0.2	122 ± 1	
$\boldsymbol{b}_{1\beta}$	13.0 ± 0.2	30 ± 1	92 ± 1

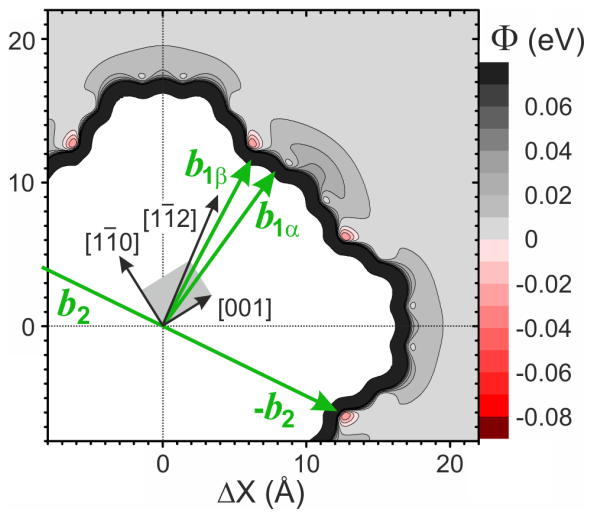

FIG. 3. Result of the pair potential calculations for two CuPc molecules of equal orientation. The interaction energy is plotted as a function of x and y offsets between the centers of the two molecules (adapted from [29]). The black arrows indicate high-symmetry directions of the Ag(110) surface; the green arrows, the unit cell vectors of the α and β superstructures.

discussed above reveal, $U_{\beta}^{m\leftrightarrow s} > U_{\alpha}^{m\leftrightarrow s}$ must hold true. This means that (i) the molecule-substrate interaction favors the α phase and (ii) at low temperatures it is the molecule-substrate interaction rather than the intermolecular interaction which determines the prevailing structure ($0 < U_{\alpha}^{m\leftrightarrow m} - U_{\beta}^{m\leftrightarrow m} < U_{\beta}^{m\leftrightarrow s} - U_{\alpha}^{m\leftrightarrow s}$) [32]. Under this premise the occurrence of the structural pattern observed in STM at low temperatures [see Fig. 2(b)] can be rationalized as a quasiperiodic release (three to five, mostly four molecular rows) of the strain that results from the heightened intermolecular repulsion in the α superstructure. We hence conclude that the appearance of two CuPc superstructures on Ag(110) is caused by a subtle balance between molecule-substrate and molecule-molecule interaction forces, resulting in two phases with similar energies, one of which (β) is slightly favored by the intermolecular, the other (α) by the interfacial attraction.

B. Electronic properties: Reduction of symmetry

Taking a closer look at constant current STM images of a CuPc monolayer [Figs. 2(b), 4(a), and 4(b)], one notices that the two pairs of opposite IIUs appear with different contrast: the IIU pair aligned closer with the Ag[1$\bar{1}$0] direction is brighter than the other pair. Thus, the original D_{4h} symmetry of CuPc is reduced to a twofold-symmetric contrast in STM. This effect is noticeably stronger when the molecules are imaged at positive bias; i.e., unoccupied molecular states are depicted. Images recorded in constant-height mode (Fig. 5) exhibit an even more strongly enhanced difference between brighter and darker IIU pairs. As mentioned above, similar symmetry reductions have already been observed in STM studies for several MPc [8–11,15].

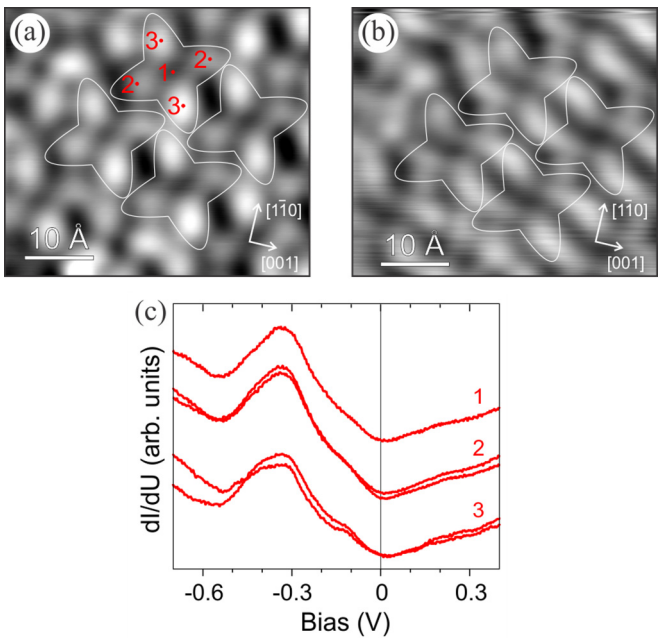

FIG. 4. Constant-current STM images of a CuPc/Ag(110) monolayer, recorded at different bias voltages: (a) $U = +0.342$ V, $I = 0.5$ nA, (b) $U = -0.300$ V, $I = 0.5$ nA. (c) Tunneling spectra recorded at different locations above a CuPc molecule. Positions are marked in panel (a): (1) at the center of the molecule, (2) at IIU$^{[001]}$, (3) at IIU$^{[1\bar{1}0]}$. For clarity, spectra are vertically shifted with respect to each other.

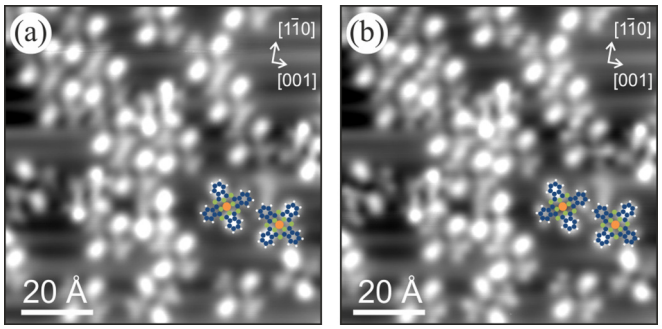

FIG. 5. Constant-height STM images of a CuPc/Ag(110) submonolayer. (a) $U = +0.05$ V, (b) $U = -0.05$ V. The current at the set point was $I = 0.75$ nA.

Interestingly, changing the sign of the bias voltage in STM does not invert the contrast ratio of the two pairs of IIUs: in both constant-current [Figs. 4(a) and 4(b)] and constant-height (Fig. 5) scanning modes the IIU pair aligned closer with the Ag[1$\bar{1}$0] (32° away) is brighter than the one aligned closer with the Ag[001] direction. From now on we will refer to them as IIU$^{[1\bar{1}0]}$ and IIU$^{[001]}$. The corresponding e_g orbitals will be labeled LUMO$^{[1\bar{1}0]}$ and LUMO$^{[001]}$ [Fig. 2(d)]. This suggests that the STM contrast difference is due to a topographic effect [11]: the darker IIU$^{[001]}$ is closer to the surface than the brighter IIU$^{[1\bar{1}0]}$.

Tunneling spectra recorded at different locations over the CuPc molecule (above its center, above IIU$^{[001]}$, and above IIU$^{[1\bar{1}0]}$) look essentially the same [Fig. 4(c)]. Regardless of the location, STS shows a single peak at approximately -0.33 V, which supposedly represents the CuPc LUMO that is occupied because of charge transfer from the metal (see below for a proof of this conjecture). Both its intensity and energy position remain almost the same across the entire molecule, even at the center of the molecule where the LUMO$^{[1\bar{1}0]}$ and LUMO$^{[001]}$ wave functions have a node [cf. Figs. 1(b) and 1(c)] and STM images indeed show a local brightness minimum [Fig. 4(a), location 1]. Thus we conclude that either the binding energies and occupations of the two e_g orbitals LUMO$^{[1\bar{1}0]}$ and LUMO$^{[001]}$ are the same, or STS happens to be insensitive to subtle differences in the local densities of states of the CuPc LUMOs. The latter might be caused by a specific feature of STS, namely that it probes molecular electronic states far away from the molecule and thus senses only the wave function tails that extend far into the vacuum.

We therefore turn to ARPES, and PT in particular, to search for differences between the LUMO$^{[1\bar{1}0]}$ and the LUMO$^{[001]}$ which might explain the symmetry reduction seen in STM (but not in STS). The angle-integrated photoelectron spectrum in Fig. 6 (solid curve) displays two occupied molecular states between the Fermi level and the Ag d band, one at approximately 0.3 eV binding energy in accordance with STS, and another one at 1.35 eV. To reveal the nature of these states, we employ the PT approach [19,20], measuring constant binding energy (CBE) maps at corresponding energies. These are displayed in Fig. 7.

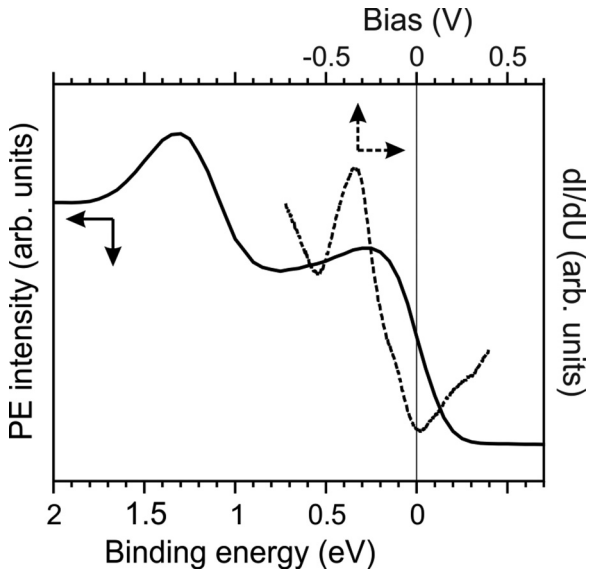

FIG. 6. Angle-integrated photoemission intensity of a CuPc/Ag(110) monolayer (solid curve), compared to the average of the tunneling spectra from Fig. 4(c) that were recorded at different locations above a single CuPc molecule (dashed curve).

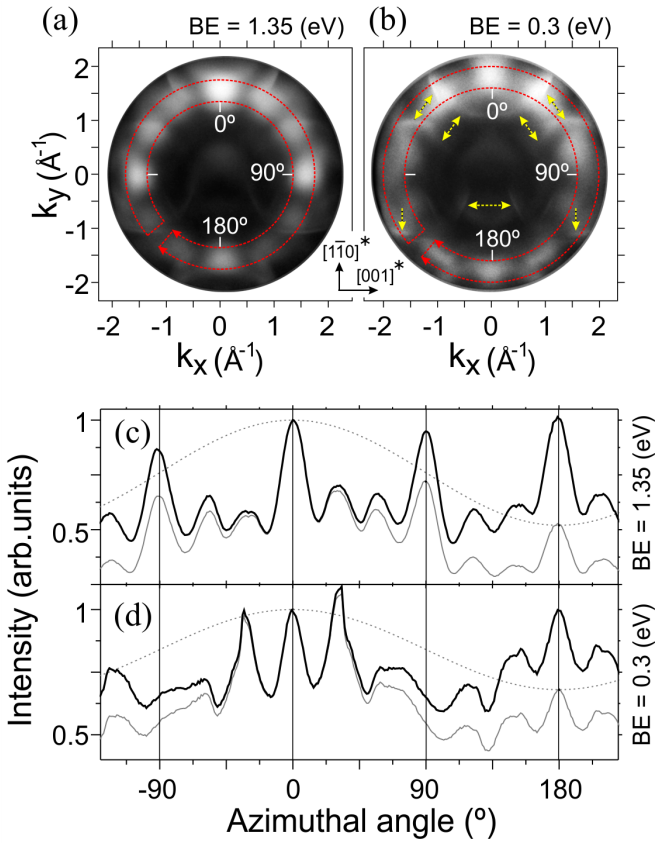

FIG. 7. (a), (b): CBE maps at binding energies of 1.35 eV and 0.3 eV. Yellow dashed arrows in (b) indicate the Ag *sp* bands. (c), (d): Corresponding photoemission intensities, integrated radially over the fraction of reciprocal space between the red circular lines, and plotted as a function of the azimuthal emission angle. Gray curve: as measured; black curve: normalized by the cosine function shown as a dotted line to correct for the polarization factor.

Note that the measured CBE maps [Figs. 7(a), 7(b), 8(m), and 8(n)] exhibit a strong forward/backward asymmetry of photoemission. This results from the experimental geometry of the NanoESCA PEEM [17], with grazing incidence of the photon beam (65° to the surface normal) and the $\boldsymbol{A}$ vector in the plane spanned by the surface normal and the photon wave vector. A corresponding $\boldsymbol{A}\cdot\boldsymbol{k}$ correction was applied to all theoretical maps, where $\boldsymbol{A}$ is the vector potential of the incident light and $\boldsymbol{k}$ the wave vector of the emitted electron [19]. To compare the theoretical CBE maps with their experimental counterparts, all prevailing molecular orientations must be taken into account. According to our structural models, both the α and β superstructures contain only molecules oriented such that their long molecular axes are rotated by $\simeq \pm 32°$ away from the high-symmetry directions [1$\bar{1}$0] and [001] of the Ag. Note that in our experiment the Ag(110) sample was aligned such that its [1$\bar{1}$0] direction lies in the same plane as the incident light and the sample normal. Therefore, two identical CBE maps calculated for a single isolated CuPc molecule are rotated by 64° relative to each other and superimposed, in order to mimic two symmetry-equivalent domains of CuPc/Ag(110). The left column of Fig. 8 illustrates this procedure for the highest occupied molecular orbital (HOMO). Panel (d) shows the calculated CBE map for the single HOMO in panel (a), properly accounting for the $\boldsymbol{A}\cdot\boldsymbol{k}$ polarization factor. Panel (j) shows the corresponding CBE map for two molecules rotated 64° relative to each other.

For the LUMO, an analogous procedure is carried out. However, we distinguish two cases: First, we assume that only one of the two initially degenerate e_g orbitals is occupied by charge transfer. In the second case, both e_g orbitals remain degenerate and are therefore occupied equally. The former case is displayed in the middle column of Fig. 8, the latter in the right column. It is apparent that in the former case the LUMO CBE map has an underlying twofold symmetry if the forward/backward asymmetry is disregarded, while in the latter case the underlying symmetry is fourfold. As we will see below, it is this difference which eventually allows us to distinguish between the two scenarios in the experiment.

Comparing experimental and theoretical CBE maps, we conclude that the photoemission peak at 1.35 eV (Fig. 6, solid curve) arises from the CuPc HOMO, since the corresponding CBE map simulated for CuPc/Ag(110) [cf. Fig. 8(j)] closely resembles the measured one at this binding energy [Figs. 7(a) and 8(m)]. Note that because of the fourfold symmetry of the CuPc HOMO, both the corresponding experimental and theoretical CBE maps of the CuPc monolayer also display a fourfold symmetry, distorted only by the $\boldsymbol{A}\cdot\boldsymbol{k}$ polarization factor. Specifically, the HOMO CBE map contains four symmetry-equivalent features at ($\pm$1.5, 0) Å^{-1} and (0, $\pm$1.5) Å^{-1} in reciprocal space, with 4 pairs of additional weaker spots at ($\pm$1.25, $\pm$0.9) Å^{-1} and ($\pm$0.9, $\pm$1.25) Å^{-1} [Fig. 7(a)]. The corresponding profile is shown in Fig. 7(c), where the photoelectron intensity is plotted along the azimuthal angle as indicated in Fig. 7(a). Note that raw data (gray curve) was normalized by a cosine function, yielding the black curve, to compensate for the forward/backward asymmetry of the experimentally observed pattern.

Having assigned the photoemission peak at 1.35 eV to the CuPc HOMO, the feature observed at $\simeq$0.3 eV must

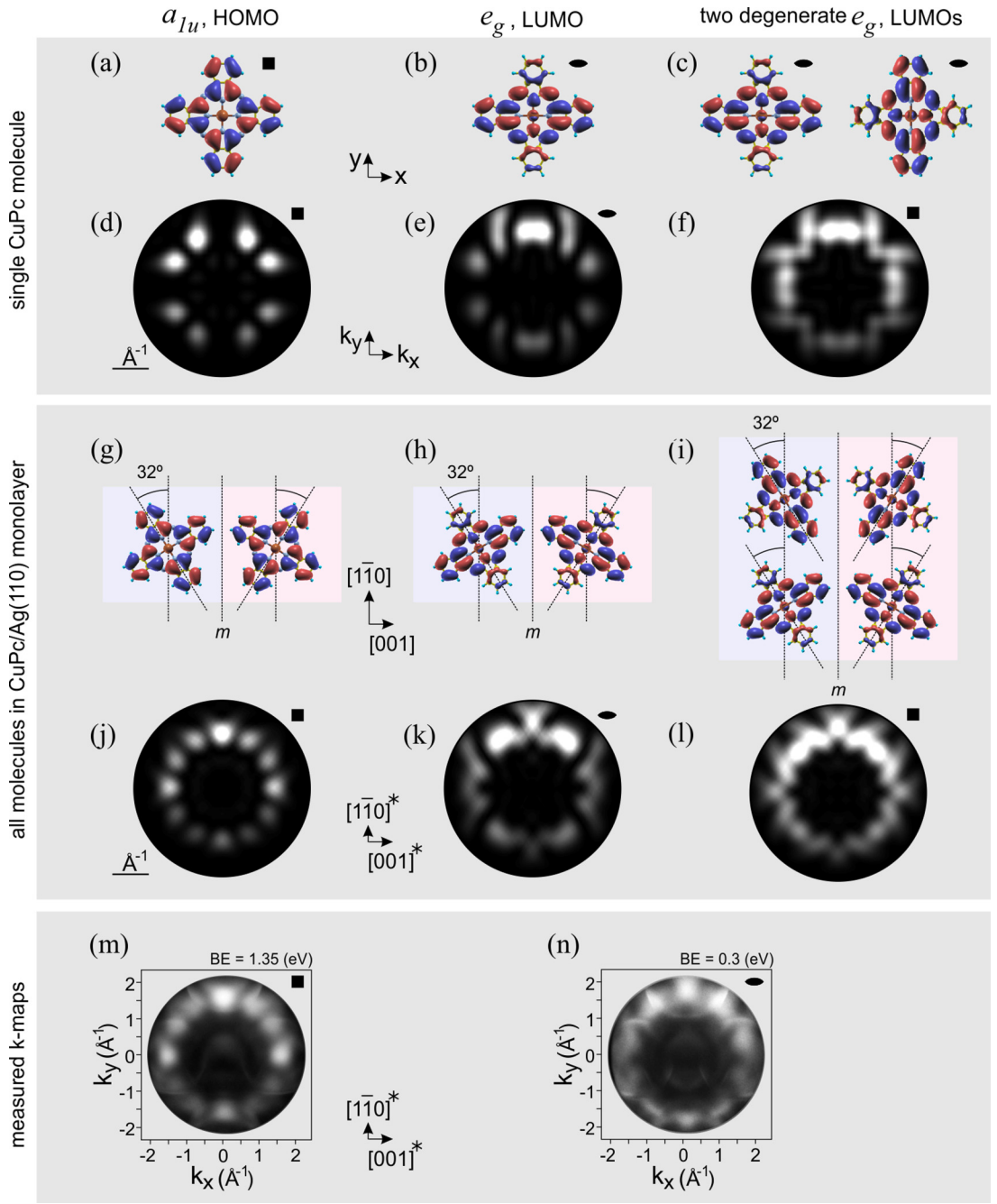

FIG. 8. (a) CuPc HOMO (calculated for the gas-phase molecule). (b) One of the CuPc LUMOs. (c) The degenerate pair of two CuPc LUMOs. Corresponding calculated CBE maps, including the polarization factor, are displayed in (d), (e), (f). (g) A pair of CuPc HOMOs, belonging to molecules in the two mirror domains of the α or β superstructures. (h) Same as in panel (g), but for LUMO$^{[001]}$. (i) Same as in panel (g), but for the degenerate pair of LUMO$^{[1\bar{1}0]}$ and LUMO$^{[001]}$. Corresponding calculated CBE maps, including the polarization factor, are displayed in (j), (k), (l). (m), (n): CBE maps measured with PEEM at binding energies of 1.35 eV and 0.3 eV, respectively. Black labels denote the twofold and fourfold underlying symmetry (excluding the backward/forward asymmetry) of the corresponding objects.

be ascribed to the LUMO, occupied due to charge transfer from the metal. However, the question still remains whether both of the initially degenerate e_g orbitals of the LUMO receive the same amount of charge, or whether there is a preferential charge transfer into only one of the two. Because of the overlap of molecular features with those of the substrate bands the analysis of the CBE map measured at $\simeq$0.3 eV [Figs. 7(b) and 8(n)] is challenging. The substrate features [marked by yellow arrows in Fig. 7(b)] arise from the *sp* band of Ag. The key observation is that the experimental CBE map in Figs. 7(b) and 8(n) lacks the underlying fourfold symmetry that is discernible in Fig. 8(l): We observe two symmetry-equivalent features at (0, $\pm$1.9) Å^{-1}, but in the perpendicular direction along k_x photoelectron intensity at the corresponding locations is absent. This rules out the scenario in which both the LUMO$^{[1\bar{1}0]}$ and the LUMO$^{[001]}$ are equally

occupied. The azimuthal intensity profiles [Figs. 7(c) and 7(d)] confirm this conclusion: While the CBE map corresponding to HOMO has 4 identical (note the $\boldsymbol{A}\cdot\boldsymbol{k}$ polarization factor) maxima in the $[1\bar{1}0]^*$, $[001]^*$, $[\bar{1}10]^*$, and $[00\bar{1}]^*$ directions, the emission at 0.3 eV exhibits twofold symmetry.

Overall, the theoretical map in Fig. 8(k), belonging to the scenario that only the $\mathrm{LUMO}^{[001]}$ receives charge from substrate [Fig. 2(d)], adequately resembles the experimental one: bright triple-spot features appear around the $[1\bar{1}0]^*$ direction at $(0,\pm(1.5\ldots2))$ Å^{-1} and much weaker W-shaped features are located at approximately $(\pm1.5, 0)$ Å^{-1}. Although the experimental map at 0.3 eV is best described by the $\mathrm{LUMO}^{[001]}$, due to its complicated contrast caused by interference with the substrate sp emissions a small contribution from the $\mathrm{LUMO}^{[1\bar{1}0]}$ cannot be excluded. We can, however, exclude with certainty that both take up an equal amount of charge, and thus have proven that the degeneracy of the two orbitals is indeed lifted upon adsorption.

Turning back to our STM data we note that the pair $\mathrm{IIU}^{[001]}$, i.e., the wings of the molecule which coincide with the $\mathrm{LUMO}^{[001]}$ that receives more charge from the metal [Fig. 2(d)], always appears darker, resulting in the well-known twofold-symmetric STM contrast [Figs. 4(a), 4(b), and 5]. At the beginning of this section, we have attributed this contrast to a topographic effect; i.e., the darker $\mathrm{IIU}^{[001]}$ is closer to the surface than the brighter $\mathrm{IIU}^{[1\bar{1}0]}$. In fact, this distortion is likely caused by a slight difference in the interaction strength between the metal and pairs $\mathrm{IIU}^{[001]}$ and $\mathrm{IIU}^{[1\bar{1}0]}$, originating in turn from the surface anisotropy: the Ag[001] direction is crystallographically more open and therefore more reactive, pulling $\mathrm{IIU}^{[001]}$ closer to the surface than $\mathrm{IIU}^{[1\bar{1}0]}$. Evidently, this initial conjecture is now corroborated by the results of our PT analysis, according to which the e_g orbital spreading over $\mathrm{IIU}^{[001]}$ receives more charge from the metal, possibly because $\mathrm{IIU}^{[001]}$ comes closer to the metal surface. Hence, this part of the CuPc molecule again appears to be more strongly involved in the chemical interaction with Ag surface. Thus, we find a synergy of topography (molecular distortion) and electronic properties (preferential charge transfer). One may speculate that the occupation of only one of the LUMOs leads to a further stabilization and/or enhancement of the substrate-induced molecular distortion by a Jahn-Teller effect.

IV. SUMMARY AND CONCLUSION

We have studied ordered monolayers of CuPc on Ag(110) by means of STM, STS, LEED, and ARPES-based photoemission tomography. We found two long-range ordered superstructures of CuPc/Ag(110): α and β. The coexistence of these superstructures is driven by a balance of intermolecular and interfacial forces. In both superstructures CuPc molecules are found to have the same orientation with respect to the Ag surface. Moreover, they appear with lower symmetry than the native symmetry of CuPc. We attribute this to the distortion of molecules: the $\mathrm{IIU}^{[001]}$ pair rotated by 32° against the [001] direction of Ag comes closer to the surface than the $\mathrm{IIU}^{[1\bar{1}0]}$ pair. Finally, ARPES-based PT proves that this bending goes hand in hand with preferential charge donation into the $\mathrm{IIU}^{[001]}$ pair, lifting of the orbital degeneracy between the two e_g orbitals making up the LUMO in gas-phase CuPc molecules. The anisotropic surface reactivity triggers the molecular distortion and the preferential charge transfer.

ACKNOWLEDGMENTS

Photoemission experiments were performed at the Elettra Sincrotrone Trieste (Italy) and supported by the European Partial Support program. D.L., P.P., and M.G.R. acknowledge financial support from the Austrian Science Fund (FWF) Projects No. P27649-N20 and No. P27427-N20. We thank I. Kröger (Physikalisch-Technische Bundesanstalt Braunschweig) for providing data for Fig. 3.

[1] J. M. Gottfried, Surf. Sci. Rep. **70**, 259 (2015).
[2] A. Kraft, R. Temirov, S. K. M. Henze, S. Soubatch, M. Rohlfing, and F. S. Tautz, Phys. Rev. B **74**, 041402 (2006).
[3] S. Duhm, A. Gerlach, I. Salzmann, B. Broker, R. Johnson, F. Schreiber, and N. Koch, Org. Electron. **9**, 111 (2008).
[4] A. Mugarza, N. Lorente, P. Ordejón, C. Krull, S. Stepanow, M.-L. Bocquet, J. Fraxedas, G. Ceballos, and P. Gambardella, Phys. Rev. Lett. **105**, 115702 (2010).
[5] N. Marom, O. Hod, G. E. Scuseria, and L. Kronik, J. Chem. Phys. **128**, 164107 (2008).
[6] D. Lüftner, M. Milko, S. Huppmann, M. Scholz, N. Ngyuen, M. Wießner, A. Schöll, F. Reinert, and P. Puschnig, J. Electron Spectrosc. Relat. Phenom. **195**, 293 (2014).
[7] N. F. Phelan and M. Orchin, J. Chem. Educ. **45**, 633 (1968).
[8] S.-H. Chang, S. Kuck, J. Brede, L. Lichtenstein, G. Hoffmann, and R. Wiesendanger, Phys. Rev. B **78**, 233409 (2008).
[9] H. Karacuban, M. Lange, J. Schaffert, O. Weingart, T. Wagner, and R. Möller, Surf. Sci. **603**, L39 (2009).
[10] Y. Wang, X. Ge, C. Manzano, J. Kröger, R. Berndt, W. A. Hofer, H. Tang, and J. Cerda, J. Am. Chem. Soc. **131**, 10400 (2009).
[11] R. Cuadrado, J. I. Cerda, Y. Wang, G. Xin, R. Berndt, and H. Tang, J. Chem. Phys. **133**, 154701 (2010).
[12] Y. Wang, J. Kröger, R. Berndt, and W. Hofer, Angew. Chem. Int. Ed. **48**, 1261 (2009).
[13] Of course, in most cases geometric and electronic effects will be coupled to each other, because a geometric distortion of the molecule caused by the external environment will also break the electronic symmetry within the molecule, and vice versa an electronic symmetry reduction will generally lead to a structural distortion (Jahn-Teller effect [18]). Yet, it is an important question to ask which is the primary and/or dominant of the two mechanisms.
[14] O. Snezhkova, J. Lüder, A. Wiengarten, S. R. Burema, F. Bischoff, Y. He, J. Rusz, J. Knudsen, M.-L. Bocquet, K. Seufert, J. V. Barth, W. Auwärter, B. Brena, and J. Schnadt, Phys. Rev. B **92**, 075428 (2015).

[15] C. Uhlmann, I. Swart, and J. Repp, Nano Lett. **13**, 777 (2013).
[16] P. Borghetti, A. El-Sayed, E. Goiri, C. Rogero, J. Lobo-Checa, L. Floreano, J. E. Ortega, and D. G. de Oteyza, ACS Nano **8**, 12786 (2014).
[17] V. Feyer, M. Graus, P. Nigge, M. Wießner, R. Acres, C. Wiemann, C. Schneider, A. Schöll, and F. Reinert, Surf. Sci. **621**, 64 (2014).
[18] H. A. Jahn and E. Teller, Proc. R. Soc. London A **161**, 220 (1937).
[19] P. Puschnig, S. Berkebile, A. J. Fleming, G. Koller, K. Emtsev, T. Seyller, J. D. Riley, C. Ambrosch-Draxl, F. P. Netzer, and M. G. Ramsey, Science **326**, 702 (2009).
[20] P. Puschnig, E.-M. Reinisch, T. Ules, G. Koller, S. Soubatch, M. Ostler, L. Romaner, F. S. Tautz, C. Ambrosch-Draxl, and M. G. Ramsey, Phys. Rev. B **84**, 235427 (2011).
[21] J. Sforzini, F. C. Bocquet, and F. S. Tautz arXiv:1609.06894.
[22] P. Bayersdorfer, http://spot-plotter.software.informer.com.
[23] C. Schneider, C. Wiemann, M. Patt, V. Feyer, L. Plucinski, I. Krug, M. Escher, N. Weber, M. Merkel, O. Renault, and N. Barrett, J. Electron Spectrosc. Relat. Phenom. **185**, 330 (2012).
[24] J. P. Perdew, K. Burke, and M. Ernzerhof, Phys. Rev. Lett. **77**, 3865 (1996).
[25] X. Gonze, B. Amadon, P.-M. Anglade, J.-M. Beuken, F. Bottin, P. Boulanger, F. Bruneval, D. Caliste, R. Caracas, M. Côté, T. Deutsch, L. Genovese, P. Ghosez, M. Giantomassi, S. Goedecker, D. Hamann, P. Hermet, F. Jollet, G. Jomard, S. Leroux, M. Mancini, S. Mazevet, M. Oliveira, G. Onida, Y. Pouillon, T. Rangel, G.-M. Rignanese, D. Sangalli, R. Shaltaf, M. Torrent, M. Verstraete, G. Zerah, and J. Zwanziger, Comput. Phys. Commun. **180**, 2582 (2009).
[26] N. Troullier and J. L. Martins, Phys. Rev. B **43**, 1993 (1991).
[27] Note that identical LEED patterns for CuPc/Ag(110) were reported by A. H. Schäfer, C. Seidel, and H. Fuchs, Adv. Func. Mater. **11**, 193 (2001). However, only one superstructure was suggested, leaving half of the observed diffraction spots unaccounted for.
[28] D. E. Hooks, T. Fritz, and M. D. Ward, Adv. Mater. **13**, 227 (2001).
[29] I. Kröger, B. Stadtmüller, C. Wagner, C. Weiss, R. Temirov, F. S. Tautz, and C. Kumpf, J. Chem. Phys. **135**, 234703 (2011).
[30] C. Kleimann, B. Stadtmüller, S. Schröder, and C. Kumpf, J. Phys. Chem. C **118**, 1652 (2014).
[31] B. Stadtmüller, C. Henneke, S. Soubatch, F. S. Tautz, and C. Kumpf, New J. Phys. **17**, 023046 (2015).
[32] See Supplemental Material at http://link.aps.org/supplemental/10.1103/PhysRevB.94.205144 for this and other aspects of the superstructure stabilization and transformation from the point of view of thermodynamics.